Water Research 289 (2026) 124799

Contents lists available at ScienceDirect

Water Research

journal homepage: www.elsevier.com/locate/watres

Mechanisms and reversibility of glyphosate and phosphorus ligands sorption on Al_2O_3: Experimental evidence and computational modeling

Mingshuai Wang [a], Liangxuan Wang [b], Philipp R. Martin [a,c], Daniel Buchner [a], Johannes Lützenkirchen [d], Alfred J. Meixner [b,*], Stefan B. Haderlein [a,*]

[a] Geo- and Environmental Research Center, Department of Geosciences, Eberhard Karls Universität Tübingen, 72076 Tübingen, Germany
[b] Institute of Physical and Theoretical Chemistry, Eberhard Karls Universität Tübingen, 72076 Tübingen, Germany
[c] Centre for Microbiology and Environmental Systems Science, Division of Environmental Geosciences, University of Vienna, 1090 Vienna, Austria
[d] Institute for Nuclear Waste Disposal, Karlsruhe Institute of Technology, 76344 Eggenstein-Leopoldshafen, Germany

HIGHLIGHTS

- Estimated Log K values for glyphosate and multi-P ligands sorbed on γ-Al_2O_3.
- SCM well models pH- and loading-dependent glyphosate/multi-P ligand complexation.
- Revealed pH-dependent energy landscape for glyphosate/phosphate sorption on Al_2O_3(110).
- DFT shows glyphosate superior stability via carboxylate monodentate at alkaline pH.
- SCM explains irreversible glyphosate/AMPA sorption in competition via monodentate.

GRAPHICAL ABSTRACT

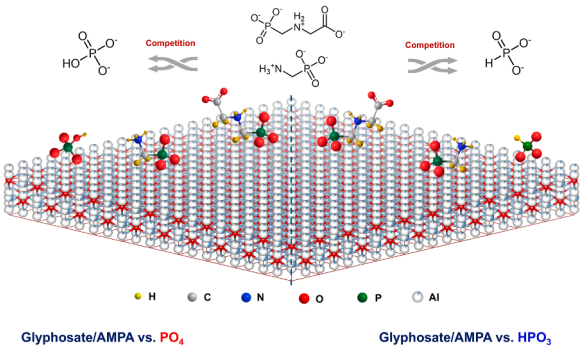

ARTICLE INFO

Keywords:
Glyphosate
AMPA
Phosphonic acid
Phosphate
SCM
DFT

ABSTRACT

The environmental fate and risk of glyphosate (Gly) are critically influenced by its retention at soil-water interfaces. While aluminum (oxyhydr)oxides (Al_2O_3, $Al(OH)_3$, AlOOH) are abundant in soils, their adsorption mechanisms for Gly have received considerably less attention than iron (hydr)oxides in geochemical modeling. This work employs a combined experimental-surface complexation model (SCM)-density functional theory (DFT) approach to systematically investigate the complexation of Gly and various phosphorus ligands (individually and competitively) on Al_2O_3. Beyond the widely studied phosphate (PO_4), we also introduce the aminomethylphosphonic acid (AMPA) and phosphonic acid (HPO_3), both containing phosphonate groups (-PO_3), into the framework. For individual adsorptions, SCM and DFT results consistently reveal pH- and loading-dependent complexation structures, comparable to iron mineral studies while filling Al_2O_3-specific knowledge gaps. DFT provides a full-pH energy analysis for Gly and PO_4 on the Al_2O_3(110) surface, specifically indicating the superior stability of Gly via carboxylate (-COO) monodentate complexation under high pH. Crucially, our SCM model, as first applied in such competitive organic-inorganic systems, identifies the adsorption irreversibility for weakly adsorbed species (Gly, AMPA) and explicitly links monodentate coordination to irreversibility at high loadings. DFT results elucidate the thermodynamic competition mechanisms at low loadings. These insights pave the way

* Corresponding authors.
E-mail addresses: alfred.meixner@uni-tuebingen.de (A.J. Meixner), stefan.haderlein@uni-tuebingen.de (S.B. Haderlein).

https://doi.org/10.1016/j.watres.2025.124799
Received 24 July 2025; Received in revised form 9 October 2025; Accepted 13 October 2025
Available online 13 October 2025

in precisely predicting and elucidating the environmental adsorption behavior of Gly at aluminum-rich soil matrix.

1. Introduction

As the most widely used herbicide globally, glyphosate (N-(phosphonomethyl)glycine, Gly) has raised significant environmental concerns due to its extensive application and potential ecological impacts. (Duke, 2020) While Gly exhibits a relatively short half-life in soil and water, its primary degradation product aminomethylphosphonic acid (AMPA) demonstrates greater environmental persistence than its parent compound. (Duke, 2020, 2011; Bento et al., 2019) Consequently, both aforementioned amino phosphonates (APs) interact strongly with mineral surfaces in environmental matrices, which mostly govern their environmental fate and mobility. Both APs tend to accumulate in soils, particularly under dry conditions, (Al-Rajab et al., 2008) and can be transported to groundwater and surface waters through various pathways including surface runoff and vertical soil transport. (Al-Rajab et al., 2008; Bento, 2018) The enhanced persistence of AMPA, combined with the adsorption-driven retention of both APs, underscores the importance of understanding their sorption behavior for assessing the long-term environmental risks of Gly-derived contamination.

Furthermore, Gly and AMPA compete for adsorption sites with naturally occurring phosphorus species, primarily phosphate (PO_4) and phosphonic acid (H_3PO_3, deprotonated to HPO_3). These competing species originate from various sources including agricultural fertilizers, household detergents, wastewater discharge, and stormwater runoff. (Zhang et al., 2022; Rott et al., 2018) PO_4 is well-documented to exhibit competitive adsorption with Gly on mineral surfaces due to their similar binding mechanisms via phosph(on)ate groups, (Gimsing et al., 2004, 2007) whereas HPO_3 has received limited research attention despite being a phosphonate structurally analogous to Gly and AMPA. Recent analytical advances (Rott et al., 2020; Armbruster et al., 2020) enabling trace-level detection of organophosphonates in environmental samples have revealed their natural occurrence in various geochemical environments. Importantly, microbial degradation of organophosphonates generates HPO_3 as a transient intermediate, while PO_4 is the ultimate mineralization product. (Sun et al., 2019; Nader et al., 2023) Therefore, investigating the environmental behavior of PO_4/HPO_3 and the competitive interactions with Gly/AMPA represents an important step that should provide insights into phosphonate fate and transport mechanisms.

Aluminum (oxyhydr)oxides (Al_2O_3, $Al(OH)_3$, AlOOH) constitute a major component of soil mineral assemblages, existing in various crystalline and amorphous forms with distinct surface properties and reactivity. (Kittrick, 2024) While corundum (α-Al_2O_3) and gibbsite (α-$Al(OH)_3$) are thermodynamically stable, (Li et al., 2013) metastable phases like boehmite (γ-AlOOH) often exhibit higher specific surface area (SSA) and adsorption reactivity, making them particularly relevant in interfacial processes. Notably, although extensive research has focused on Gly and PO_4 adsorption on iron hydroxides, (Ahmed et al., 2018; Li et al., 2023; Gustafsson and Antelo, 2022; Hiemstra and Zhao, 2016) comparative studies examining the adsorption behavior on their aluminum-counterparts remain limited. This knowledge gap represents an obvious research necessity, as the aluminum minerals may exhibit different binding mechanisms and competitive behaviors compared to iron-based minerals, potentially influencing the environmental fate of Gly in aluminum-rich soils.

The theoretical simulations offer a powerful approach to elucidate the underlying adsorption mechanisms and surface complexation reactions for various environmental contaminants. Previous density functional theory (DFT) studies have successfully determined binding configurations and energetics for Gly, (Yan and Jing, 2018; Chen et al., 2022) AMPA, (Sacanamboy et al., 2024; Wang et al., 2023) PO_4, (Ahmed et al., 2020, 2024), and HPO_3 (Luschtinetz et al., 2008; Nilsing et al., 2005) on mineral surfaces. However, the microscopic picture modelled by DFT faces limitations when applied to high-loading and multi-component competitive systems due to computational constraints and complexity in modelling electrostatic interactions. Surface complexation modeling (SCM) provides a complementary approach that can mitigate these limitations by incorporating thermodynamic principles and experimental data to predict adsorption behavior across wide ranges of pH, (Van Eynde et al., 2022; Mendez and Hiemstra, 2020) ionic strength, (Hiemstra et al., 1999; Lutzenkirchen et al., 2008) and adsorbate concentrations. (Geysels et al., 2025) Nevertheless, SCM often simplifies surface reaction mechanisms by assuming single-site adsorption. In reality, adsorption typically involves complex multi-site coordination, (Gustafsson and Antelo, 2022) multidentate complexation, (Dixit and Hering, 2006) and hydrogen bonding (Galicia-Andres et al., 2021) interactions inadequately captured by simplified SCM assumptions. Integrating SCM with molecular-level DFT insights thus offers a synergistic framework for more reliably understanding and predicting complex environmental adsorption processes.

Since previous investigations have primarily focused on single-adsorbate systems, competitive adsorption mechanisms remain challenging. This work represents the first systematic analysis of binary competitive systems (Gly/AMPA vs. PO_4/HPO_3) through an integrated experimental-SCM-DFT approach. Our comprehensive methodology enables an accurate prediction of the influence of pH variations, concentration changes, and competitive interactions on surface speciation and binding affinity. The mechanistic insights obtained from this multifaceted approach have significant environmental implications for understanding Gly fate in contaminated systems, facilitating the choice of potential remediation strategies, and assessing the long-term environmental risks associated with Gly application and its metabolite persistence, specifically in agricultural ecosystems.

2. Materials and methods

2.1. Chemicals and materials

Chemicals used in this study included glyphosate (96 %), AMPA (99 %), and phosphonic acid (H_3PO_3, 99 %), classified as phosphonates, and all purchased from Sigma Aldrich. Potassium dihydrogen phosphate (KH_2PO_4, ≥99.5 %, Merck) was used as the phosphate source. HEPES buffer (≥99.5 %, Sigma-Aldrich) was employed to maintain a stable pH of 7 in some experiments. Potassium chloride (KCl, 99.0–100.5 %, Sigma-Aldrich) served as the background electrolyte for experiments conducted at pH 4, 5, 9, and 11 in the sorption studies. All chemicals used for quantitative analysis were of analytical grade. Laboratory solutions were prepared with ultrapure water (0.057 μS/cm) (GenPure Pro UV, Thermo Fisher Scientific, Germany) and stored in a 4 °C fridge in the dark prior to use. The speciation schemes of Gly, AMPA, PO_4, and HPO_3 are presented in Fig. S1.

Commercial Al_2O_3 was obtained from Merck, with a density of 3.94 g/cm^3 at 20 °C and a Brunauer-Emmett-Teller (BET) SSA of 133.6 m^2/g (see Fig. S3). Additional detailed characterizations are provided in the SI (Fig. S4 for scanning electron microscopy images, Fig. S5 for X-ray diffractograms, and Fig. S6 and Fig. S7 for microwave plasma atomic emission spectroscopy analysis).

2.2. Batch sorption experiments

The single and binary adsorption of Gly (0.05–1 mM), AMPA (0.05–1 mM), PO_4 (0.05–1 mM), and HPO_3 (0.05–1 mM) onto Al_2O_3 (2 g/L) was

investigated through batch experiments at equilibrium pH 4, 5, 7, 9, and 11 (pH 11 only for single adsorption). All experiments were conducted in triplicate for single sorption systems and in duplicate for binary sorption systems. The react suspensions contained a background electrolyte of 0.02 M KCl. Stock solutions of adsorbates and Al_2O_3 suspensions were pre-adjusted to the target pH using HCl and KOH prior to mixing. The equivalent stock solution was then added to the suspension to achieve the desired final concentrations. For binary sorption, Gly (0.36 mM) or AMPA (0.36 mM) were pre-equilibrated with Al_2O_3 before the addition of PO_4 (0.05–2 mM) or HPO_3 (0.05- 2 mM). All samples were incubated in PP centrifugation tubes and shaken for 12 h (Kinetics study sees in Fig. S8, Table S1) on a horizontal shaker (HS 501, IKA, Germany). After sorption, the pH of each suspension was re-checked using a pH meter equipped with an ORP electrode (Seven2Go, Mettler Toledo, Switzerland), and phase separation was achieved by centrifugation at 12,000 rcf for 10 min. CO_2 was not excluded in batch experimental work to make the conditions more environmentally relevant. A Further discussion of the effect of dissolved inorganic carbon originating from the atmospheric CO_2 on adsorption is provided in the SI (Fig. S9).

The aqueous concentrations of Gly and AMPA were quantified using ion chromatography coupled with a conductivity detector (IC—CD, 883 Basic IC plus, Metrohm, Switzerland) and an electrochemical detector (IC-ECD, 930 Compact IC Flex, Metrohm, Switzerland), respectively. The IC—CD method was also applied to determine HPO_3 concentrations. Detailed descriptions of both analytical methods are provided in the SI (Fig. S10 and Fig. S11). The PO_4 concentrations were measured using an ultraviolet visible spectrophotometer (UV5Bio, Mettler Toledo, Switzerland) via the molybdenum blue method. (Murphy and Riley, 1962)

2.3. Titration and SCM of Al_2O_3

The surface properties of Al_2O_3 were characterized by acid-base titration using an automated titrator (836 Titrando, Metrohm, Switzerland). Titrations were performed with 0.01 M HCl and 0.01 M KOH as titrants, in the presence of 0.01 M or 0.1 M KCl as the background electrolyte. Each titration began by acidifying the suspension to pH 4.5 with HCl, followed by a slow back titration with KOH at a rate of 0.2 mL/min. Titrant additions were made stepwise, with the suspension equilibrating for 120 s after each increment until the pH drift stabilized below 1 mV/min. To minimize CO_2 interference, the system was continuously purged with N_2 gas. The total surface area of the solid suspension at the start of the titration exceeded 10 m^2, ensuring sufficient sensitivity. (Lützenkirchen et al., 2012) Given the mesoporous structure of Al_2O_3 (Fig. S3), which can induce titration hysteresis, (Hiemstra et al., 1999) we analyzed the impact of signal drift criteria on titration stability in the SI (Fig. S12). A series of titration data analyses (Table S2, Figs. S13, and Fig. S14) provided some important parameters for SCM, including the point of zero charge (pH_{pzc} = 8.96), estimated conditional acidity constants (pK_a = 5.27, pK_b = 12.65), and surface site density (N_s, 1.53 site/nm^2). Among these, pH_{pzc} was corroborated by zeta potential measurements (Zetasizer Nano ZSP, Malvern Panalytical, UK) via regression of zeta potential versus pH in the linear region (Fig. S15).

The charge distribution multisite complexation (CD-MUSIC) model quantitatively analyzes ligand binding affinity at the mineral/water interface by incorporating electrostatic contributions, including inner- and outer-layer capacitances within the Stern layer. Referring to the previous work by Hiemstra et al., (Hiemstra et al., 1999) the CD-MUSIC model evaluation for Al_2O_3 charge behavior is detailed in the SI (Table S3, Fig. S16). However, due to the inherent complexity of the CD-MUSIC model for Al_2O_3 and the current lack of established CD factors for the adsorption systems studied here, we employed the simpler diffuse layer model (DLM). The DLM offers a robust and widely applicable framework for interpreting macroscopic adsorption data, with greater parametric stability and reduced computational uncertainty, making it better suited to the comparative objectives of this study. As a widely adopted 2-pK formalism, the DLM describes that counterions accumulate and co-ions are depleted in the diffuse layer, with both chemical bonding and electrostatic effects (via Boltzmann factors) contributing to adsorption energies. (Dzombak and Morel, 1991) For Al_2O_3, the primary adsorption sites are singly coordinated surface groups (≡AlOH), which undergo protonation/deprotonation to form amphoteric surface species ($\equiv AlOH_2^+$ and $\equiv AlO^-$). These species interact with adsorbates to form surface complexes and deprotonated monodentate (M), deprotonated bidentate (B), protonated monodentate (MH), protonated bidentate (BH), and doubly protonated monodentate (MH_2) complexes were considered in the DLM framework. All surface complexation reactions for Gly, AMPA, PO_4, and HPO_3 (Fig. S2) and their corresponding affinity constants (log K) were optimized using Visual MINTEQ 3.1 coupled with PEST. (Gustafsson, 2011; Doherty, 2016) Atmospheric CO_2 level of 410 ppm was incorporated into all DLM simulations to account for its influence on aqueous carbonate speciation and proton balance under experimentally relevant conditions. The estimated parameters are summarized in Table 1.

2.4. DFT computational approach

All electronic structure calculations were performed at the Kohn-Sham DFT level using the CP2K/QUICKSTEP simulation package, (Kuhne et al., 2020; VandeVondele et al., 2005) in which Gaussian and plane wave (GPW) formalism is implemented. The auxiliary PW basis used to represent the valence electron density in reciprocal space has an energy cutoff of 400 Ry. In our cases, the exchange-correlation Perdew-Burke-Ernzerhof (PBE) (Perdew et al., 1996) and Bayesian Error Estimation Functional with van der Waals corrections (BEEF-vdW) (Wellendorff et al., 2012) functional were employed using the TZVP Gaussian basis set with a D3 dispersion correction. (Grimme et al., 2011, 2010) The original geometry of the unit cell of the Al_2O_3 in the bulk phase was adopted from Gu et al., (Gu et al., 2021) which was constructed according to the well-documented crystallographic data by Digne. (Digne et al., 2002, 2004) The surface was described via a slab containing a 3 × 3 supercell in the plane of the surface and the upper four layers normal to the surface. To prevent any interaction between periodically replicated slabs, 20 Å of vacuum space was added along the surface normal. The supercell of the model was fully optimized under the 2D periodic boundary conditions. Dipole correction was applied

Table 1
Estimated log K for Gly, AMPA, PO_4, and HPO_3 sorption on the coordinated surface sites of Al_2O_3. M and B refer to monodentate and bidentate complexes, respectively.

Complexation Equation	Form	log K
$\equiv AlOH + H^+ \leftrightarrow \equiv AlOH_2^+$		7.35
$\equiv AlOH - H^+ \leftrightarrow \equiv AlO^-$		-10.57
$\equiv AlOH + H^+ + Gly^{-3} \leftrightarrow \equiv AlGly^{-2} + H_2O$	M	0.25
$2\equiv AlOH + 2H^+ + Gly^{-3} \leftrightarrow \equiv Al_2Gly^{-1} + 2H_2O$	B	22.24
$\equiv AlOH + H^+ + HGly^{-2} \leftrightarrow \equiv AlHGly^{-1} + H_2O$	MH	15.55
$2\equiv AlOH + 2H^+ + HGly^{-2} \leftrightarrow \equiv Al_2HGly + 2H_2O$	BH	28.16
$\equiv AlOH + H^+ + H_2Gly^{-1} \leftrightarrow \equiv AlH_2Gly + H_2O$	MH_2	25.82
$\equiv AlOH + H^+ + H_3Gly \leftrightarrow \equiv AlH_3Gly^{+1} + H_2O$	MH_3	0.85
$\equiv AlOH + H^+ + AMPA^{-2} \leftrightarrow \equiv AlAMPA^{-1} + H_2O$	M	12.44
$2\equiv AlOH + 2H^+ + AMPA^{-2} \leftrightarrow \equiv Al_2AMPA + 2H_2O$	B	19.19
$\equiv AlOH + H^+ + HAMPA^{-1} \leftrightarrow \equiv AlHAMPA + H_2O$	MH	21.03
$2\equiv AlOH + 2H^+ + HAMPA^{-1} \leftrightarrow \equiv Al_2HAMPA^{+1} + 2H_2O$	BH	27.01
$\equiv AlOH + H^+ + H_2AMPA \leftrightarrow \equiv AlH_2AMPA^{+1} + H_2O$	MH_2	26.15
$\equiv AlOH + H^+ + PO_4^{-3} \leftrightarrow \equiv AlPO_4^{-2} + H_2O$	M	13.57
$2\equiv AlOH + 2H^+ + PO_4^{-3} \leftrightarrow \equiv Al_2PO_4^{-1} + 2H_2O$	B	27.42
$\equiv AlOH + H^+ + HPO_4^{-2} \leftrightarrow \equiv AlHPO_4^{-1} + H_2O$	MH	26.75
$2\equiv AlOH + 2H^+ + HPO_4^{-2} \leftrightarrow \equiv Al_2HPO_4 + 2H_2O$	BH	24.41
$\equiv AlOH + H^+ + H_2PO_4^{-1} \leftrightarrow \equiv AlH_2PO_4 + H_2O$	MH_2	31.90
$\equiv AlOH + H^+ + HPO_3^{-2} \leftrightarrow \equiv AlHPO_3^{-1} + H_2O$	M	12.17
$2\equiv AlOH + 2H^+ + HPO_3^{-2} \leftrightarrow \equiv Al_2HPO_3 + 2H_2O$	B	18.77
$\equiv AlOH + H^+ + H_2PO_3^{-1} \leftrightarrow \equiv AlH_2PO_3 + H_2O$	MH	18.31

along the z-direction. This correction is essential for reliably describing the electrostatic potential and electronic states of asymmetric slab systems with molecular adsorbates, as previously shown for open-shell systems on metal substrates.

Experimental and theoretical modeling on the low-index surfaces indicates that the (110) termination of γ-Al_2O_3 is the most stable and predominant surface. (Gu et al., 2021; Digne et al., 2002, 2004; Wischert et al., 2014) This surface features 75 % tetra-coordinated Al sites (Al-IV, Al-IV_{iso}) and 25 % tri-coordinated Al sites (Al-III), with a surface hydroxyl coverage of 5.9 OH/nm^2. (Gu et al., 2021) (Fig. 1a, b) In our modeling, the surface complexation schemes within the DLM framework were constructed based on the (110) plane, specifically targeting single-Al and double-Al sites to represent monodentate and bidentate ligand binding, respectively. (Fig. 1c) Considering the amphoteric nature of Al_2O_3 in aqueous solution, the variation of surface hydroxyl groups on the (110) plane at different pH values was adjusted according to the approach proposed by Wiberg. (Wiberg, 2019)

To compare the stability between different possible adsorbates, the adsorption energy E_{ads} is calculated as the difference in electronic energy between the adsorbate-surface complex $E_{Al2O3/adsorbate}$, the gas-phase molecules E_{probe}, and the clean Al_2O_3 slab $E_{Al2O3,}$ as shown in Eq. (1).

$$E_{ads} = E_{Al2O3/adsorbate} - E_{Al2O3} - E_{probe} \quad (1)$$

where E_{Al2O3} and $E_{adsorbate}$ represent the calculated total energy of the Al_2O_3 surface and adsorbate in a water solvent, respectively, the term $E_{Al2O3/adsorbate}$ denotes the total energy of the Al_2O_3 surface with adsorbate attached. A negative value signifies a stable adsorption configuration.

3. Results and discussion

3.1. Al_2O_3 surface properties and single solute sorption

Fig. 2 presents a systematic characterization of the surface properties and adsorption behavior of Al_2O_3 through a combination of experimental and modeling approaches. Fig. 2a) displays the potentiometric titration curves measured in 10 mM and 100 mM KCl electrolytes, with the intersection point defined as the pH at the point of zero charge (pH_{pzc} = 8.96). (Bourikas et al., 2003) This value was further confirmed by comparison with electrokinetic measurements (Fig. S15), demonstrating good agreement with the isoelectric point (pH_{IEP}). The DLM parameters (Section 4 in the SI) were used for subsequent surface complexation modeling. Involving electrostatic contributions, the estimated constants for formation of $\equiv AlOH_2^+$ and $\equiv AlO^-$ are 7.35 and -10.57, respectively (Table 1). The pH-dependent distribution of singly coordinated surface groups was simulated using MINTEQ (Fig. 2b). This approach allows the evaluation of pH-dependent site speciation on the (110) plane of Al_2O_3 by varying the number of surface H^+, and this information was subsequently utilized for DFT calculations. Additional comparisons of the SSA, pH_{pzc}, and N_s with literature values are provided in Table S4. Notably, the analysis of the dpH/dV curves from the titration data (Fig. S13) reveals significant dissolution of Al_2O_3 at pH below 5. This dissolution may affect the stability and charge state of surface sites, thereby influencing the acidic adsorption. A sensitivity analysis accounting for potential site loss due to dissolution (see Fig. S17) confirms that while adsorption at low pH (e.g., pH 4) may be overestimated, model predictions remain reliable across other pH ranges where no dissolution effects were observed.

Fig. 2c-f) presents the pH-dependent adsorption isotherms of Gly, AMPA, PO_4, and HPO_3 on the Al_2O_3 surface. Overall, adsorption decreases with increasing pH (4–11), primarily attributed to the reduction in positive surface charge near the pH_{pzc} (8.96), which weakens electrostatic interactions between the mineral surface and anionic adsorbates. Notably, AMPA exhibits slightly higher adsorption at pH 5 compared to pH 4 (Fig. 2d). This anomaly arises from the interplay between surface speciation and adsorbate protonation states: at pH 5, the dominant AMPA species ($HAMPA^{-1}$, ~87 %, Fig. S1) exhibits stronger electrostatic affinity for positively charged $\equiv AlOH_2^+$ sites than the predominant H_2AMPA species (~96 %, Fig. S1) at pH 4. Additionally, under acidic conditions such as pH 4, the dissolution of Al_2O_3 is enhanced (Fig. S7), releasing Al^{3+} into solution. This not only reduces the number of available surface sites but also allows dissolved Al^{3+} to form complexes with Gly or AMPA (Popov et al., 2001), thereby competing with adsorption and contributing to the observed lower uptake of AMPA at pH 4 compared to pH 5. AMPA, PO_4, and HPO_3 demonstrate higher adsorption capacities than Gly, especially under acidic to neutral conditions (pH 4–7). This observation aligns with prior reports of AMPA, PO_4 superior affinity for soil minerals. (Sidoli et al.,

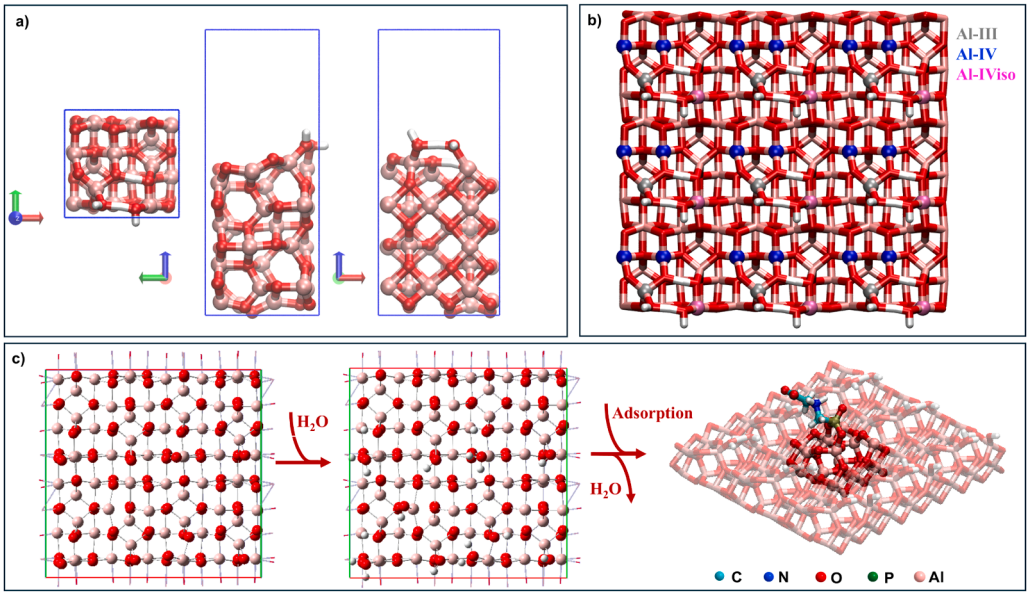

Fig. 1. a) Schematic top, front, and side view of Al_2O_3(110); **b)** Unsaturated Al atoms at the Al_2O_3(110) surface with highly-symmetrical adsorption sites labeled as Al-III, Al-IV, and Al-IV_{iso}; **c)** The surface hydroxylation of Al_2O_3(110) with a density of 5.9 OH/nm^2, along with the construction of the corresponding adsorption model.

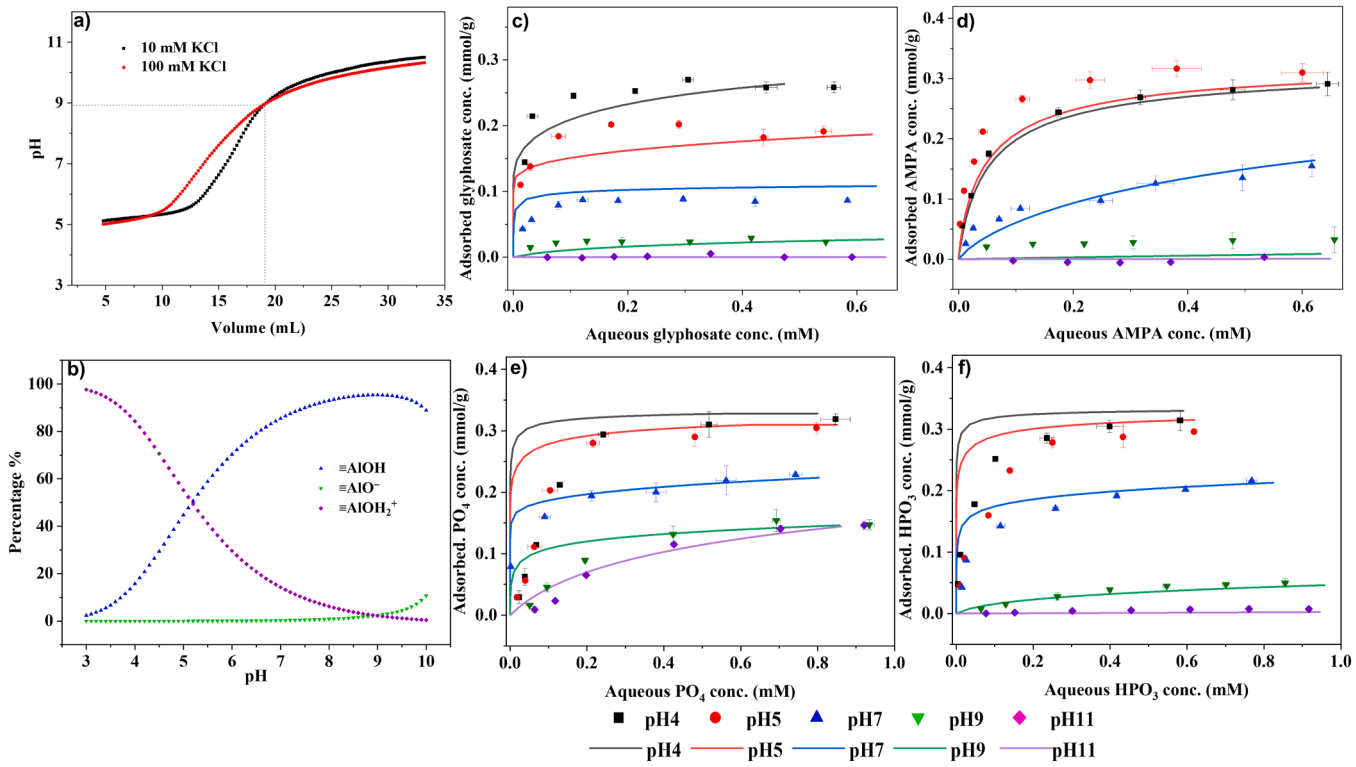

Fig. 2. $A_{l2}O_3$ in KCl: **a)** Acid-base titration at 10, 100 mM. **b)** simulated pH dependences for the species of singly coordinated surface groups. Sorption isotherms of **c)** Gly, **d)** AMPA, **e)** PO_4, and **f)** HPO_3 at pH 4, 5, 7, 9, and 11 on Al_2O_3. Dots are experimental results, and solid lines are simulated results.

2016; Gimsing et al., 2004; Munira et al., 2018) The enhanced adsorption of zwitterionic AMPA (similar to Gly) and HPO_3 may stem from their smaller molecular sizes, which reduce steric hindrance, and their reliance on phosphonate group (-PO_3) mediated surface complexation – *a* mechanism shared with Gly. (Gimsing and Borggaard, 2002; Wimmer et al., 2022) The experimental points show good agreement with DLM simulations (evaluated by R^2 in the SI, Table S6), confirming model reliability in predicting surface complexation across diverse chemical conditions. These comprehensive datasets provide input for understanding contaminant adsorption mechanisms in Al_2O_3-dominated environmental systems. Additional simulations of surface complexation corresponding to these isotherms are detailed in Fig. S18-Fig. S21, and the sites occupied during adsorption, as calculated from experimental data, are compared with DLM-applied N_s in Table S5.

3.2. *Surface complexation of single solute sorption*

The modeling parameters listed in Table 1 enable the calculation of

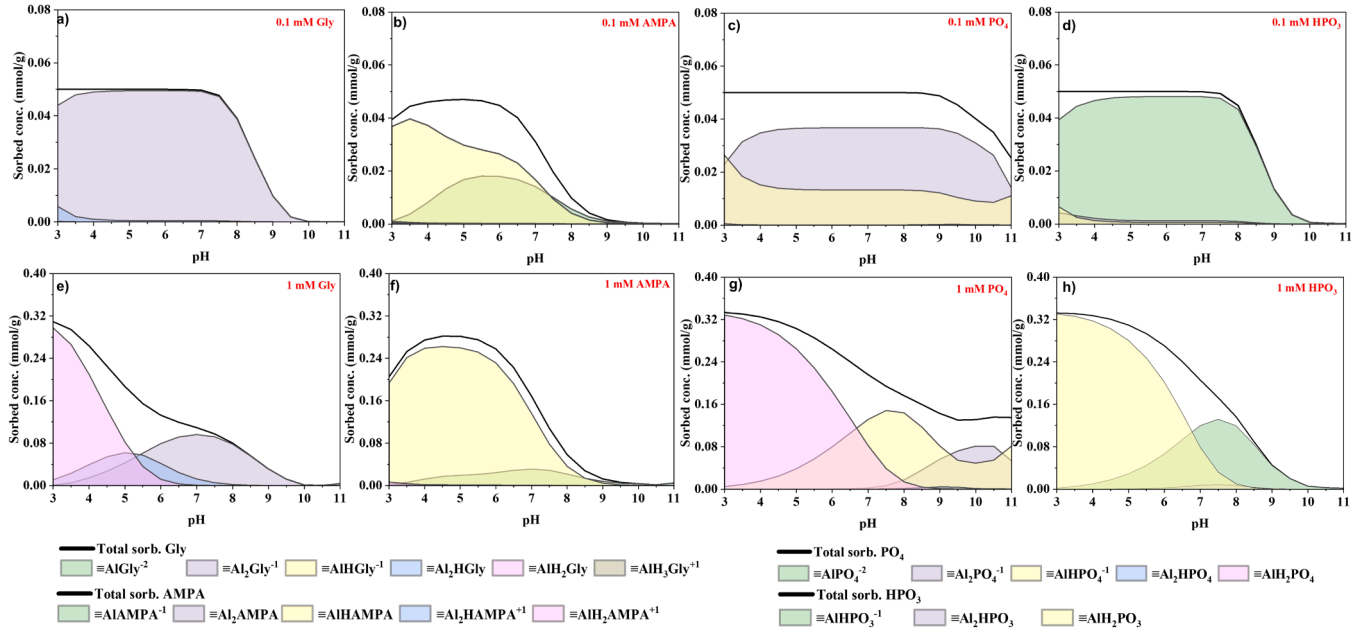

Fig. 3. Simulated adsorption edges and surface complexations of Gly, AMPA, PO_4, and HPO_3 on Al_2O_3 at initial conc. of **a-d)** 0.1 mM and **e-h)** 1 mM.

surface speciation for Gly, AMPA, PO_4, and HPO_3 complexes on the Al_2O_3 as functions of pH and initial concentration. Fig. 3a–d) and Fig. 3e–h) illustrate adsorption behaviors at representative initial concentrations of 0.1 mM (low loading) and 1 mM (high loading).

Our model suggests that Gly primarily forms a B-type complex with the Al_2O_3 surface under low-loading conditions. With increasing loading, BH and particularly MH_2 demonstrate enhanced formation under acidic conditions (Fig. 3a, e). While no direct comparisons exist for Gly adsorption on Al_2O_3, recent SCM studies on goethite by Geyseis and Hiemstra (Geysels et al., 2025) show predominant B-type formation (>60 %), consistent with our findings. Complementary DFT calculations (Yan and Jing, 2018) are commensurate with predominant B-type Gly complexation on goethite at acidic pH. Similarly, PO_4 adsorption on Al_2O_3 exhibits B-type dominance at low loadings, while MH and MH_2 species prevail at higher concentrations (Fig. 3b and f). Early NMR studies (Johnson et al., 2002; Kim and Kirkpatrick, 2004) suggested mixed inner-sphere and outer-sphere PO_4 complexes on γ-Al_2O_3, while multimodal characterization and DFT analysis (Li et al., 2013) later identified bridging bidentate surface complexes on α-Al_2O_3 across pH 3–11. Despite our focus on γ-Al_2O_3 (Fig. S5), low-loading complexation patterns align with observations on α-Al_2O_3. Notably, this work demonstrates M-type complex dominance over B-type configurations for both Gly and PO_4 under high-loading conditions.

In contrast, AMPA and HPO_3 exhibit more pronounced M and MH-type contributions even at low loadings. As shown in Fig. 3b), MH complexes dominate AMPA adsorption with secondary M-type contributions. At high concentrations (Fig. 3f), MH species maintain predominance in AMPA uptake. Though no reports on the AMPA/ Al_2O_3 system, Barja's comparative study with Gly on goethite (Barja and Dos Santos Afonso, 2005) corroborates preferential monodentate inner-sphere binding for AMPA at acidic pH. Fig. 3d, h) reveals HPO_3 M-type dominance at low loadings on Al_2O_3, with *MH species* gaining prominence under high-loading conditions. Among related findings, Luschtinetz et al. employed DFT to analyze mono-, bi-, and tridentate HPO_3 adsorption modes on hydroxylated alumina surfaces, but were unable to identify the most favorable adsorption mode. (Luschtinetz et al., 2008) Our work provides complementary insights into loading-dependent HPO_3 adsorption across two concentration regimes. For all studied adsorbates, surface complexation patterns on Al_2O_3 exhibit clear concentration dependence: monodentate configurations become increasingly dominant under high-loading conditions. According to the analysis of adsorption site occupations (Table S5), it is mechanistically linked to single-site saturation.

The DLM modelling results suggest that adsorbate binding mechanisms on Al_2O_3 are interlinked by environmental pH and initial concentration, thereby supplementing the current understanding of mineral adsorption processes.

3.3. Computational results on Gly, PO_4 sorption

The DFT computations focused on the individual adsorption behaviors of Gly and PO_4 molecules on the Al_2O_3(110) plane. The predominant surface species were determined by comparing adsorption energies, and the changes in the surface speciation during competitive adsorption were subsequently inferred by integrating experimental and SCM results. The modeling at neutral pH was based on the characteristics of Al_2O_3 and the adsorbates. Adsorption energies were calculated using two exchange-correlation functionals: PBE and BEEF-vdW. The optimized adsorption configurations for Gly and PO_4 are illustrated in Fig. S22 and Fig. S23, respectively.

Table 2 lists the calculated adsorption energies (E_{ads}) of Gly on the Al_2O_3 (110) plane at pH 7. At this pH, dissolved Gly predominantly exists as the $HGly^{-2}$ species (~99 %; Fig. S1). Given the three different Al sites (Al-III, Al-IV, and Al-IV_{iso}, Fig. 1) present on the (110) plane, the carboxyl group (-COO) and -PO_3 of $HGly^{-2}$ can form six distinct monodentate complexes. Furthermore, geometric constraints permit the -PO_3 to form three distinct bidentate complexes bridging the Al site pairs of Al-III_Al-IV, Al-III_Al-IV_{iso}, and Al-IV_Al-IV. Notably, the most negative E_{ads} corresponded to bidentate complexes, suggesting that bidentate coordination is energetically more favorable and thus dominates Gly adsorption. The H_2Gly^{-1} comprises about 1 % of Gly species at pH 7 (Fig. S1). Its complexes are exclusively monodentate and were excluded from further consideration. Among the monodentate configurations, complexes formed via the -PO_3 exhibited consistently more negative E_{ads} than those formed via the -COO. This provides direct energetic evidence supporting literature reports that Gly coordinates primarily to mineral surfaces through its -PO_3. (Sheals et al., 2002; Barja and Dos Santos Afonso, 2005) At pH 7, dissolved PO_4 mainly exists as HPO_4^{-2} (~60 %)

Table 2
Adsorption energies of Gly and PO_4 on Al_2O_3(110) at pH7. Calculations were performed using the D3BJ-PBE and BEEF-vdW functionals with the MOLOPT-TZVP basis set. Three Al sites (Al-III, Al-IV, Al-IV_{iso}) and two types of binding motifs (-COO; -PO_3) were considered for the Gly ($HGly^{-2}$ species) configurations. $H_2PO_4^{-1}$ and HPO_4^{-2} species were included to account for various PO_4 configurations.

Sorbate	Configuration	D3BJ-PBE-MOLOPT-TZVP			BEEF-vdW-MOLOPT-TZVP		
		E_{ads} (Hartree)	E_{ads} (eV)	E_{ads} (kcal/mol)	E_{ads} (Hartree)	E_{ads} (eV)	E_{ads} (kcal/mol)
Gly	Al-III_COO	−0.14	−3.81	−87.91	−0.14	−3.87	−89.20
	Al-IV_COO	−0.12	−3.34	−77.05	−0.12	−3.30	−76.21
	Al-IV_{iso}_COO	−0.14	−3.76	−86.74	−0.15	−3.96	−91.30
	Al-III_PO_3	−0.15	−4.10	−94.55	−0.14	−3.85	−88.80
	Al-IV_PO_3	−0.14	−3.81	−87.75	−0.13	−3.66	−84.39
	Al-IV_{iso}_PO_3	−0.15	−4.12	−95.01	−0.15	−4.06	−93.60
	Al-III_Al-IV_PO_3	−0.23	−6.32	−145.73	−0.22	−5.94	−137.06
	Al-III_Al-IV_{iso}_PO_3	−0.25	−6.81	−157.07	−0.26	−7.09	−163.42
	Al-IV_Al-IV_PO_3	−0.21	−5.73	−132.21	−0.21	−5.61	−129.47
PO_4	Al-III_HPO_4	−0.26	−6.97	−160.62	−0.25	−6.78	−156.37
	Al-IV_HPO_4	−0.25	−6.90	−159.13	−0.24	−6.41	−147.89
	Al-IV_{iso}_HPO_4	−0.30	−8.09	−186.46	−0.26	−6.95	−160.24
	Al-III_Al-IV_HPO_4	−0.34	−9.27	−213.84	−0.33	−8.91	−205.55
	Al-III_Al-IV_{iso}_HPO_4	−0.40	−10.92	−251.82	−0.39	−10.71	−247.07
	Al-IV_Al-IV_HPO_4	−0.31	−8.50	−195.95	−0.30	−8.25	−190.30
	Al-III_H_2PO_4	−0.12	−3.28	−75.68	−0.12	−3.18	−73.41
	Al-IV_H_2PO_4	−0.16	−4.33	−99.76	−0.10	−2.68	−61.86
	Al-IV_{iso}_H_2PO_4	−0.08	−2.13	−49.15	−0.11	−3.04	−70.04
	Al-III_Al-IV_H_2PO_4	−0.16	−4.33	−99.94	−0.15	−4.08	−94.16
	Al-III_Al-IV_{iso}_H_2PO_4	−0.20	−5.57	−128.48	−0.19	−5.04	−116.24
	Al-IV_Al-IV_H_2PO_4	−0.14	−3.80	−87.57	−0.13	−3.55	−81.77

and $H_2PO_4^{-1}$ (~40 %) (Fig. S1). The E_{ads} values of both species on the Al_2O_3(110) plane are given in Table 2. Each species can form three monodentate and three bidentate complexes on accessible Al sites. Among them, The E_{ads} values of HPO_4^{-2} complexes were generally more negative than those of $H_2PO_4^{-1}$ complexes. Considering its higher abundance (~60 %), HPO_4^{-2} plays a significant role in PO_4 adsorption on the (110) plane. Moreover, bidentate complexes consistently exhibited the most negative E_{ads} for both species, indicating that bidentate coordination is also dominant for PO_4 adsorption.

The adsorption behavior in natural systems is regulated by pH through its influence on surface speciation and mineral surface charge. (Yan and Jing, 2018; Geysels et al., 2025) To investigate the pH-dependent surface complexation of Gly and PO_4 on Al_2O_3, we calculated E_{ads} for their dominant species under acidic (pH 4) and alkaline (pH 11) conditions. The amphoteric behavior of the alumina surface was explicitly accounted for in our DFT models by adjusting the protonation states of surface hydroxyl groups. While this approach (Wiberg, 2019) captures pH-dependent surface dissociation, it does not include the effects of potential bulk dissolution at extreme pH values, which may influence site availability under strongly acidic conditions.

In aqueous solution, Gly primarily exists as H_2Gly^{-1} (~88 %, Fig. S1) at pH 4 and as Gly^{-3} (~84 %, Fig. S1) at pH 11. Adsorption energy calculations for monodentate and bidentate complexes of these species are summarized in Table 3. Similar to the neutral pH, bidentate complexes under acidic conditions exhibited greater stability, with -PO_3 monodentate configurations showing consistently lower E_{ads} compared to -COO counterparts. Notably, although bidentate complexes remain energetically favored in alkaline pH simulations, monodentate adsorption is dominated by -COO coordination. This shift might be attributed to the -COO mostly determining Gly net charge at high pH, (Galicia-Andres et al., 2021) thus resulting in stronger interactions with surface Al sites compared to the -PO_3. Nevertheless, comparative analysis of E_{ads} for Gly at pH 4, 7, and 11 confirms bidentate coordination as the dominant adsorption configuration, consistent with DLM simulations at low loading (0.1 mM, Fig. 2a). For dissolved PO_4, the dominant species are $H_2PO_4^{-1}$ (~99 %, Fig. S1) at pH 4 and HPO_4^{-2} (~89 %, Fig. S1) at pH 11. As shown in Table 3, bidentate complexes at acidic conditions display the same energetic advantage as at neutral pH. However, at pH 11, the energy difference between monodentate and bidentate configurations diminished significantly. This finding aligns with DLM simulations (0.1 mM, Fig. 2c), which indicate the co-existence of mono- and bidentate PO_4 complexes on Al_2O_3 across pH 3–11, with bidentate species generally dominant but contributing almost equally to monodentate forms at pH 11. Moreover, although the uptake of both solutes decreases with increasing pH, the corresponding adsorption energies indicate higher adsorption affinities at elevated pH.

The consistency among DFT, DLM, and experimental results highlights the reliability of our theoretical modeling. DFT calculations offer a solid microscopic description of the configurations and energetics of different surface complexation, while the DLM framework provides an intuitive macroscopic perspective on high-loading adsorption behaviors. Such hybrid modelling bridges atomistic and phenomenological insights, enabling a comprehensive understanding of surface complexation mechanisms across multiple scales.

Table 3
Adsorption energies of Gly and PO_4 on Al_2O_3(110) at acidic and alkaline pH. Calculations were performed using the D3BJ-PBE functionals with the MOLOPT-TZVP basis set. Three Al sites (Al-III, Al-IV, Al-IV_{iso}) and two types of binding motifs (-COO; -PO_3) were considered for the Gly (Gly^{-3}, $HGly^{-2}$ species) configurations. $H_2PO_4^{-1}$and HPO_4^{-2} species were included to account for various PO_4 configurations.

Sorbate	Main species	Configuration	D3BJ-PBE-MOLOPT-TZVP		
			E_{ads} (Hartree)	E_{ads} (eV)	E_{ads} (kcal/mol)
Gly	**Acidic pH (H_2Gly^{-1})**	Al-III_COO	−0.11	−2.96	−68.34
		Al-IV_COO	−0.09	−2.56	−59.04
		Al-IV_{iso}_COO	−0.07	−1.91	−44.06
		Al-III_PO_3	−0.13	−3.41	−78.74
		Al-IV_PO_3	−0.13	−3.65	−84.09
		Al-IV_{iso}_PO_3	−0.11	−2.95	−68.01
		Al-III_Al-IV_PO_3	−0.13	−3.60	−82.95
		Al-III_Al-IV_{iso}_PO_3	−0.22	−6.11	−140.84
		Al-IV_Al-IV_PO_3	−0.18	−4.87	−112.36
	Alkaline pH (Gly^{-3})	Al-III_COO	−0.61	−16.72	−385.49
		Al-IV_COO	−0.34	−9.16	−211.30
		Al-IV_{iso}_COO	−0.37	−10.19	−234.91
		Al-III_PO_3	\	\	\
		Al-IV_PO_3	\	\	\
		Al-IV_{iso}_PO_3	\	\	\
		Al-III_Al-IV_PO_3	−0.57	−15.57	−359.12
		Al-III_Al-IV_{iso}_PO_3	−0.57	−15.57	−359.09
		Al-IV_Al-IV_PO_3	\	\	\
PO_4	**Acidic pH ($H_2PO_4^{-1}$)**	Al-III_H_2PO_4	−0.1461	−3.98	−91.7
		Al-IV_H_2PO_4	−0.1446	−3.93	−90.72
		Al-IV_{iso}_H_2PO_4	−0.1258	−3.42	−78.91
		Al-III_Al-IV_H_2PO_4	−0.4351	−11.84	−273
		Al-III_Al-IV_{iso}_H_2PO_4	−0.2172	−5.91	−136.29
		Al-IV_Al-IV_H_2PO_4	−0.1724	−4.69	−108.2
	Alkaline pH (HPO_4^{-2})	Al-III_HPO_4	−0.4179	−11.37	−262.26
		Al-IV_HPO_4	−0.6508	−17.71	−408.39
		Al-IV_{iso}_HPO_4	−0.3475	−9.46	−218.05
		Al-III_Al-IV_HPO_4	−0.4278	−11.64	−268.48
		Al-III_Al-IV_{iso}_HPO_4	−0.4636	−12.62	−290.94
		Al-IV_Al-IV_HPO_4	−0.4531	−12.33	−284.31

* \ indicates the calculation for the configuration failed at alkaline pH.

3.4. Binary competitive sorption: Gly/ampa vs. PO_4/HPO_3

In real world systems, glyphosate typically occurs together with other compounds containing phosphorus ligands. These may subsequently compete for sorption sites on minerals. In the following, we explore such competitive adsorption scenarios. Experiments commenced by equilibrating Gly/AMPA adsorption on Al_2O_3 at a series of pH (4, 5, 7, 9), after which different amounts of PO_4/HPO_3 were added to assess competitive adsorption. The experimental results are shown in Fig. 4a,c,e,g). While the DLM simulation cannot explicitly account for possible effects of the addition order in competitive adsorption, we investigated the effect of the addition sequence experimentally (see SI, Fig. S24, Fig. S25). The results consistently reveal that, in this study, the adsorption order had a minimal effect on the competition between Gly/AMPA and PO_4/HPO_3. Specifically, Fig. S25 indicates that both sequential and simultaneous addition of competitors led to comparable adsorption outcomes for Gly. Therefore, the DLM-simulated competitive adsorption results shown in Fig. 4b,d,f,h) can be directly compared with the corresponding experimental data.

In the competitive adsorption system on Al_2O_3, the uptake of all four adsorbates decreased with increasing pH. However, PO_4/HPO_3 consistently exhibited stronger affinity than Gly/AMPA across all pH conditions, indicating that inorganic phosph(on)ate species possess stronger retention over APs in environmental contexts. Notably, the model accurately predicted the final adsorption states for the strongly competing adsorbates but exhibited deviations in simulating the adsorption behavior of APs. Experimentally, even in the presence of strongly adsorbing PO_4/HPO_3, APs retained partial adsorption on Al_2O_3 and were not completely desorbed, whereas the DLM model predicted complete desorption of APs under competitive conditions. This suggests that some APs surface complexes retain irreversibility, which models may underestimate sorption due to non-labile binding. This interpretation is further supported by the desorption kinetics shown in Fig. S26, where both Gly and AMPA reached a release plateau within 10 h, confirming that the irreversible fraction stems from the formation of stable complexes with Al_2O_3 rather than slow desorption kinetics.

To gain deeper insight into the desorption behavior, we examined to

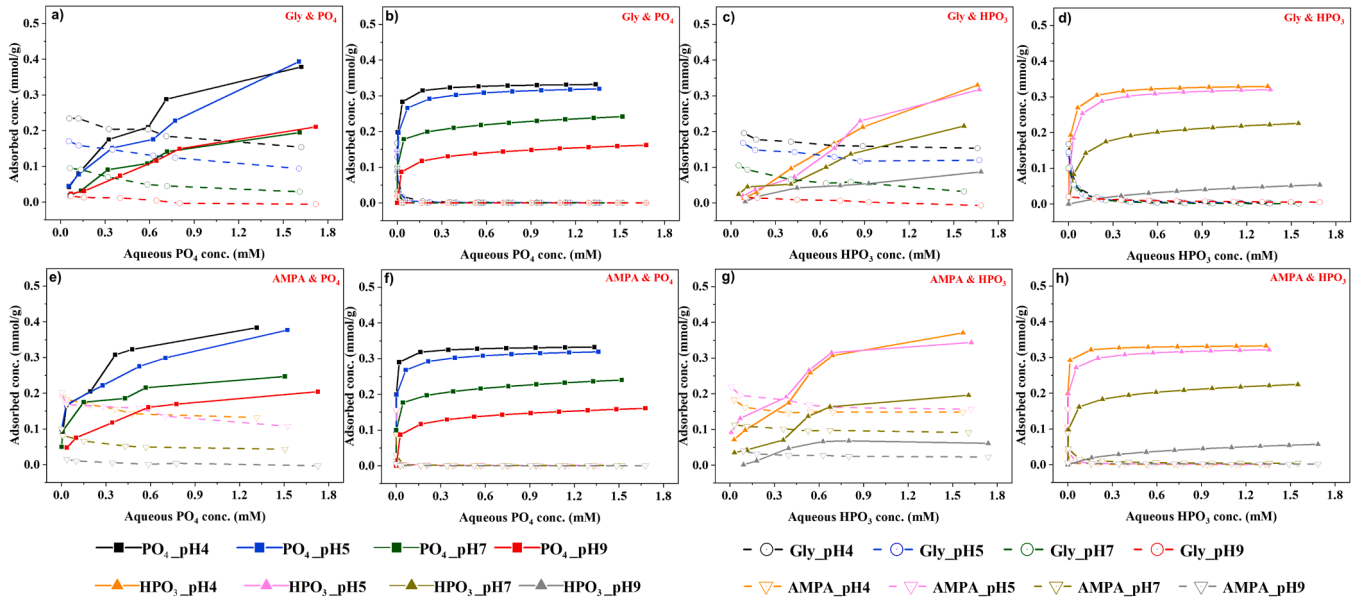

Fig. 4. Competitive binary sorption at pH4, 5, 7, and 9: **a, b)** Gly vs. PO_4, **c, d)** Gly vs. HPO_3, **e, f)** AMPA vs. PO_4, **g, h)** AMPA vs. HPO_3 on Al_2O_3. **a, c, e, g)** are experimental results, and **b, d, f, h)** are simulated results.

what extent these compounds can be removed from the Al_2O_3 surface by repeatedly replacing the background electrolyte. As shown in Fig. S27, even in the absence of competing adsorbates, these compounds could not be completely desorbed from the mineral surface at neutral pH, confirming their partially irreversible adsorption. Therefore, Gly and AMPA adsorbed on such mineral surfaces will probably exhibit persistence in natural environments, which then would influence their removal as well as potential degradation processes.

3.5. *Surface complexation of binary competitive sorption*

The surface complexation simulations in Fig. 5 provide critical clues for the model underestimation of Gly/AMPA adsorption in binary systems. Specifically, in 0.1 mM competitive systems (Fig. 5a-d), measurable adsorption competition persists between Gly/AMPA and PO_4/HPO_3, while their complexation patterns under various pH conditions remain largely consistent in single-solute systems. However, in the Gly-PO_4 competition system, PO_4 exhibits altered surface species distribution under acidic pH, where both MH and B complexes contribute almost equally. Cross-referencing with the DFT-calculated binding energy data in Table 3, we hypothesize that pre-equilibrated Gly maintains partial B-type coordination sites (Al-III_AIViso_PO_3 = -6.11 eV) that resist replacement by PO_4 in a bidentate mode(Al-III_AIViso_H_2PO_4 = -5.91 eV), thereby reducing the B-type dominance of PO_4. At higher concentrations (1 mM, Fig. 5e-f), PO_4/HPO_3 retains its original adsorption modes and complexation mechanisms. Conversely, Gly/AMPA exhibits altered complexation behavior concomitant with a dramatic reduction in uptake. The model predicts a transition of dominant

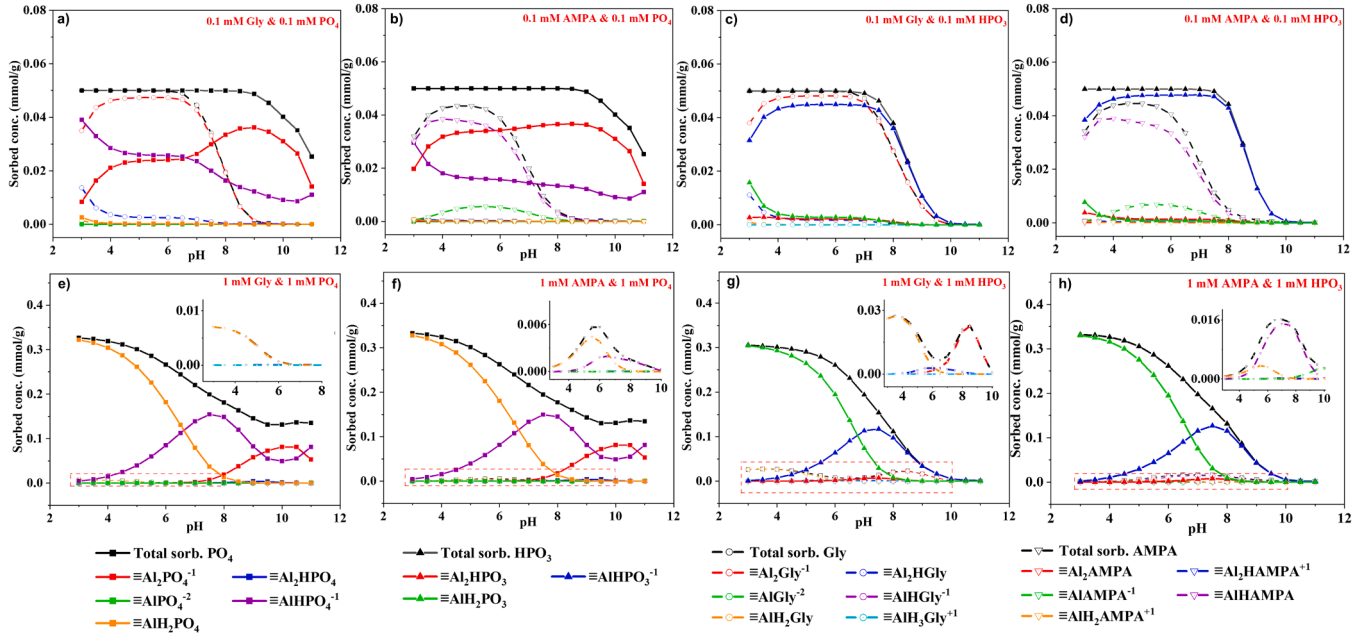

Fig. 5. Simulated adsorption edges and surface complexations of **a, e)** Gly vs. PO_4 **b, f)** AMPA vs. PO_4 **c, g)** Gly vs. HPO_3 **d, h)** AMPA vs. HPO_3 on Al_2O_3 at initial conc. of 0.1 mM and 1 mM.

AMPA surface species to MH/MH_2-type complexes under these conditions, while Gly shows MH_2 dominance when competing with PO_4, but comparable MH_2 and B contributions when competing with HPO_3. Notably, experimental studies on competitive surface complexation involving Al_2O_3, particularly between Gly/AMPA and PO_4/HPO_3, remain scarce. Earlier spectroscopic work (Waiman et al., 2016) suggested that the presence of PO_4 on goethite does not alter the fundamental nature of Gly adsorption, and recommended SCM modeling as a reliable tool for predicting the competitive speciations. Our simulations align with and extend this approach, indicating that monodentate complexes of Gly and AMPA serve as the key irreversible surface species for these compounds on Al_2O_3 surfaces at high loadings.

4. Conclusions

Our combined experimental-SCM-DFT approach provides molecular-level insights into the binding of Gly and multiple phosphorus ligands to Al_2O_3, considering environmental key factors such as pH and co-solutes and thereby filling a knowledge gap for Al_2O_3 while extending interpretations comparable to prior iron mineral studies. The model accurately predicts the pH- and loading-dependent individual and competitive adsorption of Gly and various phosphorus ligands. Crucially, this study is the first to identify irreversibility for weakly adsorbed species in competitive organic-inorganic systems, specifically linking monodentate complexation to irreversibility under high loading. DFT calculations on the Al_2O_3(110) plane agree with SCM simulations and provide energetic interpretations of competitive adsorption mechanisms.

Given the abundance and ubiquity of aluminum (oxy)hydroxides in natural environments, they are key regulators of Gly retention and transport at soil-water interfaces. Our model aids in explaining the environmental fate of Gly and extends predictive capability from single species to competitive adsorption, providing a foundation for developing complex multi-component adsorption models. Furthermore, the adsorption irreversibility of Gly and AMPA suggests greater environmental persistence and, subsequently, a potentially lower bioavailability and transformation; this also extends the implications to assess the long-term retention of various organophosphonates in soils. Future studies should extend these findings to environmentally relevant micromolar concentrations, which are currently limited by analytical techniques, and include comprehensive DFT comparisons across other Al_2O_3 crystallographic planes.

CRediT authorship contribution statement

Mingshuai Wang: Writing – review & editing, Writing – original draft, Visualization, Validation, Software, Methodology, Investigation, Formal analysis, Data curation. **Liangxuan Wang:** Writing – review & editing, Visualization, Software, Methodology. **Philipp R. Martin:** Writing – review & editing, Conceptualization. **Daniel Buchner:** Writing – review & editing, Conceptualization. **Johannes Lützenkirchen:** Writing – review & editing, Supervision, Methodology. **Alfred J. Meixner:** Writing – review & editing, Supervision. **Stefan B. Haderlein:** Writing – review & editing, Supervision, Conceptualization.

Declaration of competing interest

The authors declare that they have no known competing financial interests or personal relationships that could have appeared to influence the work reported in this paper.

Acknowledgments

The authors thank Dr. Johannes Gierschner for fruitful discussion on DFT calculations, Dr. Jeremiah Shuster for SEM imaging, Tsz Ho Chiu for BET and XRD measurements, and Dr. Anna Röhnelt for MP-AES assistance. This research was supported by the China Scholarship Council (CSC). The authors acknowledge support by the state of Baden-Württemberg through bwHPC and the German Research Foundation (DFG) through grants no INST 40/575–1 FUGG (JUSTUS 2 cluster) and HA 3453/17–1.

Supplementary materials

Supplementary material associated with this article can be found, in the online version, at doi:10.1016/j.watres.2025.124799.

Data availability

No data was used for the research described in the article.

References

Ahmed, A.A., Gypser, S., Freese, D., Leinweber, P., Kühn, O., 2020. Molecular level picture of the interplay between pH and phosphate binding at the goethite–water interface. Phys. Chem. Chem. Phys. 22 (45), 26509–26524.
Ahmed, A.A., Leinweber, P., Kuhn, O., 2018. Unravelling the nature of glyphosate binding to goethite surfaces by ab initio molecular dynamics simulations. Phys. Chem. Chem. Phys. 20 (3), 1531–1539.
Ahmed, A.A., Morshedizad, M., Kühn, O., Leinweber, P., 2024. Deciphering competitive interactions: phosphate and organic matter binding on goethite through experimental and theoretical insights. Sci. Total. Environ. 940.
Al-Rajab, A.J., Amellal, S., Schiavon, M., 2008. Sorption and leaching of 14C-glyphosate in agricultural soils. Agron. Sustainable Dev. 28 (3), 419–428.
Armbruster, D., Rott, E., Minke, R., Happel, O., 2020. Trace-level determination of phosphonates in liquid and solid phase of wastewater and environmental samples by IC-ESI-MS/MS. Anal. Bioanal. Chem. 412 (20), 4807–4825.
Barja, B.C., Dos Santos Afonso, M., 2005. Aminomethylphosphonic acid and glyphosate adsorption onto goethite: a comparative study. Environ. Sci. Technol. 39 (2), 585–592.
Bento, C.P.M., 2018. Glyphosate and Aminomethylphosphonic Acid (AMPA) Behavior in Loess Soils and Off-Site Transport Risk Assessment. Wageningen University and Research.
Bento, C.P.M., van der Hoeven, S., Yang, X., Riksen, M., Mol, H.G.J., Ritsema, C.J., Geissen, V., 2019. Dynamics of glyphosate and AMPA in the soil surface layer of glyphosate-resistant crop cultivations in the loess Pampas of Argentina. Environ. Pollut. 244, 323–331.
Bourikas, K., Vakros, J., Kordulis, C., Lycourghiotis, A., 2003. Potentiometric mass titrations: experimental and theoretical establishment of a new technique for determining the point of zero charge (PZC) of metal (hydr)oxides. J. Phys. Chem. B 107 (35), 9441–9451.
Chen, P., Song, D., Zhang, X., Xie, Q., Zhou, Y., Liu, H., Xu, L., Chen, T., Rosso, K.M., 2022. Understanding competitive phosphate and silicate adsorption on goethite by connecting batch experiments with density functional theory calculations. Environ. Sci. Technol. 56 (2), 823–834.
Digne, M., Sautet, P., Raybaud, P., Euzen, P., Toulhoat, H., 2002. Hydroxyl groups on γ-alumina surfaces:: A DFT study. J. Catal. 211 (1), 1–5.
Digne, M., Sautet, P., Raybaud, P., Euzen, P., Toulhoat, H., 2004. Use of DFT to achieve a rational understanding of acid-basic properties of γ-alumina surfaces. J. Catal. 226 (1), 54–68.
Dixit, S., Hering, J.G., 2006. Sorption of Fe(II) and As(III) on goethite in single- and dual-sorbate systems. Chem. Geol. 228 (1–3), 6–15.
Doherty, J.E., 2016. Model-independent parameter estimation user manual part II: PEST utility support software. Watermark. 268.
Duke, S.O., 2011. Glyphosate degradation in Glyphosate-resistant and -susceptible crops and weeds. J. Agr. Food Chem. 59 (11), 5835–5841.
Duke, S.O., 2020. Glyphosate: environmental fate and impact. Weed. Sci. 68 (3), 201–207.
Dzombak, D.A., Morel, F.M., 1991. Surface Complexation Modeling: Hydrous Ferric Oxide. John Wiley & Sons.
Galicia-Andres, E., Tunega, D., Gerzabek, M.H., Oostenbrink, C., 2021. On glyphosate-kaolinite surface interactions. A molecular dynamic study. Eur. J. Soil. Sci. 72 (3), 1231–1242.
Geysels, B., Hiemstra, T., Groenenberg, J.E., Comans, R.N.J., 2025. Glyphosate binding and speciation at the water-goethite interface: a surface complexation model consistent with IR spectroscopy and MO/DFT. Water. Res. 273, 123031.
Gimsing, A.L., Borggaard, O.K., 2002. Competitive adsorption and desorption of glyphosate and phosphate on clay silicates and oxides. Clay. Miner. 37 (3), 509–515.
Gimsing, A.L., Borggaard, O.K., Bang, M., 2004. Influence of soil composition on adsorption of glyphosate and phosphate by contrasting Danish surface soils. Eur. J. Soil. Sci. 55 (1), 183–191.
Gimsing, A.L., Szilas, C., Borggaard, O.K., 2007. Sorption of glyphosate and phosphate by variable-charge tropical soils from Tanzania. Geoderma 138 (1–2), 127–132.
Grimme, S., Antony, J., Ehrlich, S., Krieg, H., 2010. A consistent and accurate ab initio parametrization of density functional dispersion correction (DFT-D) for the 94 elements H-Pu. J. Chem. Phys. 132 (15), 154104.

Grimme, S., Ehrlich, S., Goerigk, L., 2011. Effect of the damping function in dispersion corrected density functional theory. J. Comput. Chem. 32 (7), 1456–1465.
Gu, J., Wang, J., Leszczynski, J., 2021. Single site Fe on the (110) surface of gamma-Al(2)O(3): insights from a DFT study including the periodic boundary approach. Phys. Chem. Chem. Phys. 23 (12), 7164–7177.
Gustafsson, J.P., 2011. Visual MINTEQ 3.0 User Guide. KTH, Department of Land and Water Recources, Stockholm, Sweden, p. 550.
Gustafsson, J.P., Antelo, J., 2022. Competitive arsenate and phosphate adsorption on ferrihydrite as described by the CD-MUSIC model. ACS. Earth. Space Chem. 6 (5), 1397–1406.
Hiemstra, T., Yong, H., Van Riemsdijk, W.H., 1999. Interfacial charging phenomena of aluminum (hydr)oxides. Langmuir. 15 (18), 5942–5955.
Hiemstra, T., Zhao, W., 2016. Reactivity of ferrihydrite and ferritin in relation to surface structure, size, and nanoparticle formation studied for phosphate and arsenate. Environ. Sci-Nano 3 (6), 1265–1279.
Johnson, B.B., Ivanov, A.V., Antzutkin, O.N., Forsling, W., 2002. P nuclear magnetic resonance study of the adsorption of phosphate and phenyl phosphates on γ-Al2O3. Langmuir. 18 (4), 1104–1111.
Kim, Y., Kirkpatrick, R.J., 2004. An investigation of phosphate adsorbed on aluminium oxyhydroxide and oxide phases by nuclear magnetic resonance. Eur. J. Soil. Sci. 55 (2), 243–251.
Kittrick, J.A., 2024. Soil minerals in the Al2O3-SiO2-H2O system and a theory of their formation. Clays Clay Miner 17 (3), 157–167.
Kuhne, T.D., Iannuzzi, M., Del Ben, M., Rybkin, V.V., Seewald, P., Stein, F., Laino, T., Khaliullin, R.Z., Schutt, O., Schiffmann, F., Golze, D., Wilhelm, J., Chulkov, S., Bani-Hashemian, M.H., Weber, V., Borstnik, U., Taillefumier, M., Jakobovits, A.S., Lazzaro, A., Pabst, H., Muller, T., Schade, R., Guidon, M., Andermatt, S., Holmberg, N., Schenter, G.K., Hehn, A., Bussy, A., Belleflamme, F., Tabacchi, G., Gloss, A., Lass, M., Bethune, I., Mundy, C.J., Plessl, C., Watkins, M., VandeVondele, J., Krack, M., Hutter, J., 2020. CP2K: an electronic structure and molecular dynamics software package - Quickstep: efficient and accurate electronic structure calculations. J. Chem. Phys. 152 (19), 194103.
Li, W., Pierre-Louis, A.-M., Kwon, K.D., Kubicki, J.D., Strongin, D.R., Phillips, B.L., 2013. Molecular level investigations of phosphate sorption on corundum (α-Al2O3) by 31P solid state NMR, ATR-FTIR and quantum chemical calculation. Geochim. Cosmochim. Acta 107, 252–266.
Li, X., Yang, P., Zhao, W., Guo, F., Jaisi, D.P., Mi, S., Ma, H., Lin, B., Feng, X., Tan, W., Wang, X., 2023. Adsorption mechanisms of glyphosate on ferrihydrite: effects of Al substitution and aggregation State. Environ. Sci. Technol. 57 (38), 14384–14395.
Luschtinetz, R., Oliveira, A.F., Frenzel, J., Joswig, J.O., Seifert, G., Duarte, H.A., 2008. Adsorption of phosphonic and ethylphosphonic acid on aluminum oxide surfaces. Surf. Sci. 602 (7), 1347–1359.
Lutzenkirchen, J., Boily, J.F., Gunneriusson, L., Lovgren, L., Sjoberg, S., 2008. Protonation of different goethite surfaces–unified models for NaNO3 and NaCl media. J. Colloid. Interface Sci. 317 (1), 155–165.
Lützenkirchen, J., Preočanin, T., Kovačević, D., Tomišić, V., Lövgren, L., Kallay, N., 2012. Potentiometric titrations as a tool for surface charge determination. Croatica Chemica Acta 85 (4), 391–417.
Mendez, J.C., Hiemstra, T., 2020. Ternary complex formation of phosphate with Ca and Mg ions binding to ferrihydrite: experiments and mechanisms. Acs Earth Space Chem 4 (4), 545–557.
Munira, S., Farenhorst, A., Akinremi, W., 2018. Phosphate and glyphosate sorption in soils following long-term phosphate applications. Geoderma 313, 146–153.
Murphy, J., Riley, J.P., 1962. A modified single solution method for the determination of phosphate in natural waters. Anal. Chim. Acta 27, 31–36.
Nader, W., Zahm, A., Jaschik, J., 2023. Phosphonic acid in plant-based food and feed products – Where does it come from? Food Control 150, 109701.
Nilsing, M., Lunell, S., Persson, P., Ojamäe, L., 2005. Phosphonic acid adsorption at the TiO2 anatase (101) surface investigated by periodic hybrid HF-DFT computations. Surf. Sci. 582 (1–3), 49–60.
Perdew, J.P., Burke, K., Ernzerhof, M., 1996. Generalized gradient approximation made simple. Phys. Rev. Lett. 77 (18), 3865–3868.
Popov, K., Rönkkömäki, H., Lajunen, L.H.J., 2001. Critical evaluation of stability constants of phosphonic acids (IUPAC technical report). Pure Appl. Chem. 73 (10), 1641–1677.
Rott, E., Happel, O., Armbruster, D., Minke, R., 2020. Influence of wastewater discharge on the occurrence of PBTC, HEDP, and aminophosphonates in sediment, suspended matter, and the aqueous phase of rivers. Water. (Basel) 12 (3), 803.
Rott, E., Steinmetz, H., Metzger, J.W., 2018. Organophosphonates: a review on environmental relevance, biodegradability and removal in wastewater treatment plants. Sci. Total. Environ. 615, 1176–1191.
Sacanamboy, D.S., Quispe-Corimayhua, L., Tilvez, E.A., Yañez, O., 2024. Adsorption of aminomethylphosphonic acid on pristine graphene and graphene doped with transition metals: a theoretical study. Chem. Phys. Lett. 850, 141481.
Sheals, J., Sjoberg, S., Persson, P., 2002. Adsorption of glyphosate on goethite: molecular characterization of surface complexes. Environ. Sci. Technol. 36 (14), 3090–3095.
Sidoli, P., Baran, N., Angulo-Jaramillo, R., 2016. Glyphosate and AMPA adsorption in soils: laboratory experiments and pedotransfer rules. Environ. Sci. Pollut. Res. Int. 23 (6), 5733–5742.
Sun, M., Li, H., Jaisi, D.P., 2019. Degradation of glyphosate and bioavailability of phosphorus derived from glyphosate in a soil-water system. Water. Res. 163, 114840.
Van Eynde, E., Hiemstra, T., Comans, R.N.J., 2022. Interaction of Zn with ferrihydrite and its cooperative binding in the presence of PO4. Geochim. Cosmochim. Acta 320, 223–237.
VandeVondele, J., Krack, M., Mohamed, F., Parrinello, M., Chassaing, T., Hutter, J., 2005. QUICKSTEP: fast and accurate density functional calculations using a mixed gaussian and plane waves approach. Comput. Phys. Commun. 167 (2), 103–128.
Waiman, C.V., Arroyave, J.M., Chen, H., Tan, W., Avena, M.J., Zanini, G.P., 2016. The simultaneous presence of glyphosate and phosphate at the goethite surface as seen by XPS, ATR-FTIR and competitive adsorption isotherms. Colloids Surf., A 498, 121–127.
Wang, M., Rivenbark, K.J., Phillips, T.D., 2023. Adsorption and detoxification of glyphosate and aminomethylphosphonic acid by montmorillonite clays. Environ. Sci. Pollut. Res. Int. 30 (5), 11417–11430.
Wellendorff, J., Lundgaard, K.T., Mogelhoj, A., Petzold, V., Landis, D.D., Norskov, J.K., Bligaard, T., Jacobsen, K.W., 2012. Density functionals for surface science: exchange-correlation model development with bayesian error estimation. Phys. Rev. B 85 (23), 235149.
Wiberg, E., 2019. Lehrbuch Der Anorganischen Chemie. Walter de Gruyter GmbH & Co KG.
Wimmer, B., Neidhardt, H., Schwientek, M., Haderlein, S.B., Huhn, C., 2022. Phosphate addition enhances alkaline extraction of glyphosate from highly sorptive soils and aquatic sediments. Pest. Manage Sci. 78 (6), 2550–2559.
Wischert, R., Florian, P., Copéret, C., Massiot, D., Sautet, P., 2014. Visibility of Al surface sites of γ-alumina: a combined computational and experimental point of view. J. Phys. Chem. C 118 (28), 15292–15299.
Yan, W., Jing, C., 2018. Molecular insights into glyphosate adsorption to goethite gained from ATR-FTIR, two-dimensional correlation spectroscopy, and DFT study. Environ. Sci. Technol. 52 (4), 1946–1953.
Zhang, Q., Wang, Y., Zhang, C., Yao, Y., Wang, L., Sun, H., 2022. A review of organophosphate esters in soil: implications for the potential source, transfer, and transformation mechanism. Environ. Res. 204 (Pt B), 112122.